

RESEARCH ARTICLE

Open Access



Properties of STAT1 and IRF1 enhancers and the influence of SNPs

Mohamed Abou El Hassan^{1,2,3†}, Katherine Huang^{1†}, Manoj B. K. Eswara¹, Zhaodong Xu¹, Tao Yu¹, Arthur Aubry¹, Zuyao Ni^{1,6}, Izzy Livne-bar¹, Monika Sangwan¹, Mohamad Ahmad¹ and Rod Bremner^{1,4,5*}

Abstract

Background: STAT1 and IRF1 collaborate to induce interferon- γ (IFN γ) stimulated genes (ISGs), but the extent to which they act alone or together is unclear. The effect of single nucleotide polymorphisms (SNPs) on in vivo binding is also largely unknown.

Results: We show that IRF1 binds at proximal or distant ISG sites twice as often as STAT1, increasing to sixfold at the MHC class I locus. STAT1 almost always bound with IRF1, while most IRF1 binding events were isolated. Dual binding sites at remote or proximal enhancers distinguished ISGs that were responsive to IFN γ versus cell-specific resistant ISGs, which showed fewer and mainly single binding events. Surprisingly, inducibility in one cell type predicted ISG-responsiveness in other cells. Several dbSNPs overlapped with STAT1 and IRF1 binding motifs, and we developed methodology to rapidly assess their effects. We show that in silico prediction of SNP effects accurately reflects altered binding both in vitro and in vivo.

Conclusions: These data reveal broad cooperation between STAT1 and IRF1, explain cell type specific differences in ISG-responsiveness, and identify genetic variants that may participate in the pathogenesis of immune disorders.

Background

IFN γ is a pleiotropic cytokine that plays essential roles in antiviral and anticancer immune responses (reviewed in [1, 2]). IFN γ binds to its receptor complex and activates receptor-associated JAK kinases, which phosphorylate a substantial fraction of cytoplasmic signal transducer and activator of transcription 1 (STAT1). Phosphorylated STAT1 forms homodimers that translocate to the nucleus and bind IFN γ activation sites (GAS). STAT1 recruits histone acetyltransferases (HATs) and other transcriptional co-activators to acetylate chromatin and facilitate transcription. Genomic studies showed that STAT1 binds at promoter proximal and distal sites, suggesting a role in remote gene regulation [3–6]. Indeed, IFN γ induces long range interactions between STAT1-bound enhancers and target promoters [7–9].

Interferon regulatory factor 1 (*IRF1*) is a primary target gene of STAT1. Like STAT1, IRF1 also acts as a transcription factor (TF), binding to IRF-E motifs and interferon-stimulated response elements (ISRE) [10, 11]. Access of both STAT1 and IRF1 to target enhancers requires the SWI/SNF chromatin remodeling complex to counter PRC2, which uses the histone methyl transferase EZH2 to deposit H3K27me3 and block the induction of many other cytokine and cytokine responsive loci [7, 12, 13]. IRF1 functions at the transcription initiation level by facilitating RNA Pol II recruitment to ISGs promoters [14, 15]. IRF1 also binds to remote enhancers of the *CIITA* locus that loop together to form a 3D interconnected hub with the promoter [7]. Indeed, ChIP-chip and ChIP-seq studies show that IRF1 binds many remote enhancers [6, 16–18], and analysis of 128 transcription factors in K562 cells revealed that STAT1-IRF1 co-binding is a recurring pattern in IFN γ treated cells [19]. Notably, STAT1 is essential but not sufficient for gene induction [11], and both STAT1 and IRF1 are required for the IFN γ -induced expression of *CIITA*, *GBP1*, and *gp19* [14, 15, 20]. In addition, STAT1 complexes with

*Correspondence: bremner@lunenfeld.ca

[†]Mohamed Abou El Hassan and Katherine Huang contributed equally to this work

¹ Lunenfeld Tanenbaum Research Institute, Mt Sinai Hospital, Toronto, ON, Canada

Full list of author information is available at the end of the article



IRF1 at the *LMP2* promoter and maintains its constitutive expression [21].

Here, we studied the extent of STAT1 and IRF1 cooperation in HeLa cells within ISG-rich chromosomal segments encompassing ~10% of all known ISGs. Most of these loci responded to IFN γ in HeLa cells, leaving ~20% resistant ISGs. IRF1 binding sites outnumbered STAT1 sites 2 to 1. A large fraction of STAT1/IRF1 binding occurred at remote sites and looping studies confirmed the functional role of putative enhancers at the *SOCS1* locus. Most STAT1 binding occurred at or near to IRF1 sites (dual binding), but IRF1 often bound isolated from STAT1. Dual STAT1 and IRF1 but not isolated IRF1 or STAT1 binding was linked to ISG responsiveness. Finally, several variants affecting STAT1/IRF1 motifs induce or impair binding.

Results

Diverse gene responses to IFN γ

To define patterns of TF binding around ISGs, we employed tiling arrays to focus on 16 Mb distributed across 11 distinct chromosomal segments with a high density of ISGs (Fig. 1a, Additional file 1: Table S1). Nine segments were 1 Mb genomic regions on six chromosomes centered on specific IFN γ target genes (e.g. 1 Mb around *IRF1* etc.). Two others included a 2 Mb segment centered on *CIITA*, and a 5 Mb segment covering the complete classical 3.6 Mb MHC locus and an additional 1.4 Mb 5' region including much of the so-called extended MHC class I region (Fig. 1a; Additional file 1: Table S1). Within these regions 25% (95/375) of the genes are known ISGs, ~5 \times more than the genome-wide ISG frequency (1167/24996 ISGs) and ~15-fold above the average ISGs density per Mb. The total number of Ref-seq genes and UCSC Known Genes in the 16 Mb regions is 394 (Additional file 1: Table S1). Of these, 95% (375) were represented on the Illumina-12 Human WG-6v3 array used to assess gene expression (see below). The frequency of Refseq genes across the genome is ~6/Mb, but most of the 11 chromosomal segments in our study were gene dense (average 24/Mb), especially at the MHC (35/Mb), PSME (39/Mb) and IFITM clusters (45/Mb) (Additional file 1: Table S1). There are also 126 pseudogenes across the 16 Mb, with most (93) located at the MHC cluster (Additional file 1: Table S1). Pseudogenes are not represented on the Illumina genome wide array we used to study expression.

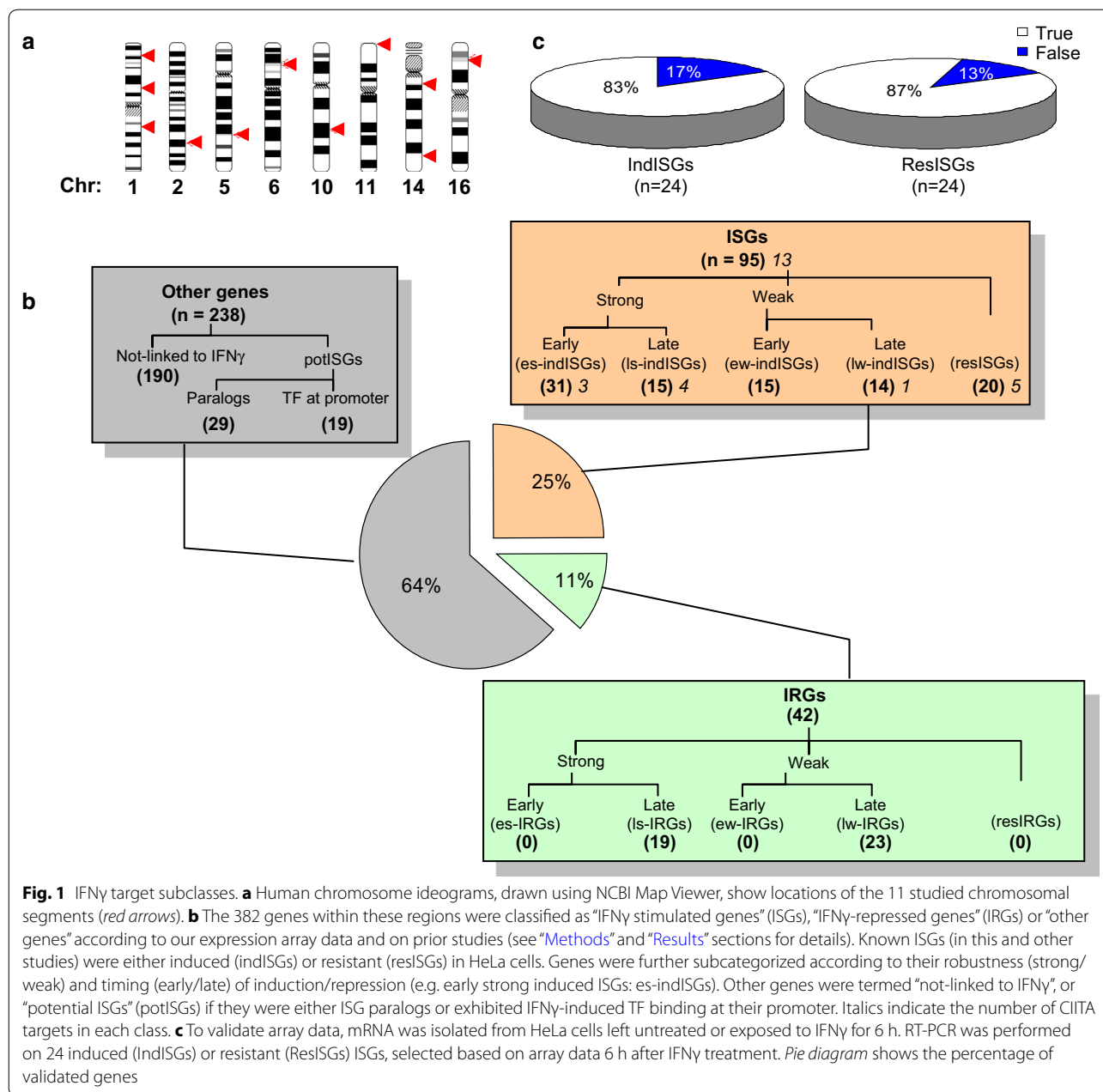
Signaling pathway target loci show cell-specific responsiveness, but the exact TF binding patterns that distinguish induction versus resistance in a specific cell type are unclear. Thus, we compared the pattern of STAT1 and IRF1 binding at different gene types. For this we compiled a database of ~ all known ISGs using our own and

prior transcriptome data (Additional file 1: Table S2). As summarized in Fig. 1b, ISGs fell into 8 classes depending on whether IFN γ caused induction, no effect (resistant ISGs in HeLa cells), or repression, and whether induction/repression were early (detected at 6 h) or late (24 or 48 h), and strong (differential score ≥ 13 , and \geq twofold change) or weak (differential score ≥ 13 , < twofold). The microarray expression data was validated using reverse transcription and quantitative PCR (RT-qPCR), which confirmed 83% (20/24) of indISGs and 87% (21/24) of resISGs (Fig. 1c). Of all 95 known ISGs on the array, 31 (33%) genes were es-indISGs, 15 (16%) were ls-indISGs, 29 (31%) were ew-indISGs or lw-indISGs, and 20 were resISGs (Fig. 1b). Es-indISGs were distributed at an average density of 1.9/Mb within the studied regions (Additional file 1: Table S1). The highest density was observed at the IFIT and GBP clusters with an average of 4.0 es-indISGs/Mb.

No genes were repressed (IFN γ repressed genes, IRGs) at the early 6 h time point, while 19 and 23 were strongly or weakly repressed at later times, respectively (ls-IRGs and lw-IRGs; Fig. 1b), suggesting indirect regulation of IRGs (perhaps through activation of a repressor). The remaining genes that were not IFN γ -responsive either in this or any prior study were termed "Other Genes". In summary, known ISGs fall into induced and resistant subclasses in HeLa cells, providing a useful system to define STAT1 and IRF1 binding patterns linked to responsiveness.

Validation of STAT1 and IRF1 ChIP-chip analyses

ChIP-chip was used to locate STAT1 and IRF1 sites at promoter proximal and distal sites of the genes of each category. STAT1 and IRF1 ChIPs were performed on chromatin from HeLa cells that were either untreated or exposed to IFN γ for 6 h. Hybridization intensities were normalized to internal standards and values from quadruplicate spots were averaged. Significantly different intensities between ChIP DNA and input DNA samples in three biological replicates ($p < 0.0001$) were determined using the Wilcoxon rank sum test. Peaks representing the significantly enriched DNA regions ($p < 0.0001$) where the ratio of ChIP to input DNA was ≥ 1.5 -fold were visualized in the UCSC browser and plotted on a log₂ scale. Only 2 STAT1 and 28 IRF1 peaks were identified in untreated cells, rising to 92 and 196 post-IFN γ treatment, respectively. Browser views are shown in Additional file 2: Figure S1 and can be visualized at [http://research.lunenfeld.ca/IFN \$\gamma\$](http://research.lunenfeld.ca/IFNgamma) . ChIP-qPCR validated 91% (20/22) and 96% (23/24) of STAT1 and IRF1 ChIP-chip peaks, respectively (Fig. 2). We compared STAT1 binding at 6 h (this study) with IFN γ -induced STAT1 binding after 30 min [22], also assessed in HeLa

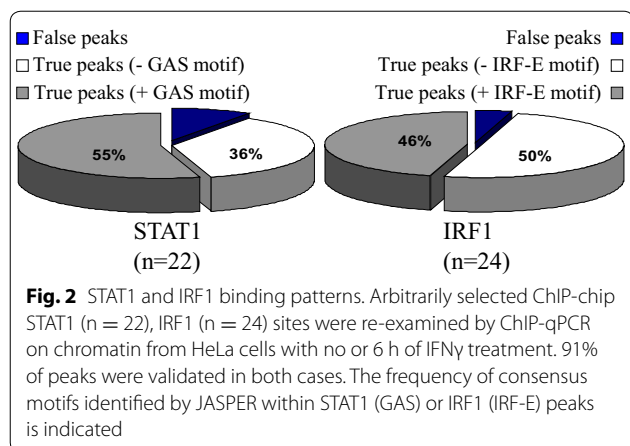


cells. In the 16 Mb of DNA assessed here, the latter study detected 26 STAT1 sites, of which 21 overlapped with the 92 STAT1 sites we detected.

Basal TF binding

Unphosphorylated STAT1 has roles in regulating ISGs days after IFN treatment [23, 24], but its role in untreated cells is less clear, although STAT1 nuclear cytoplasmic shuttling occurs even in untreated cells [25–27]. Basal STAT1 binding is linked to the nuclear localization of unphosphorylated STAT1 and contributes to the constitutive expression of some targets [21, 28]. IRF1 is also

expressed to low levels in unstimulated HeLa cells [7] and it cooperates with STAT1 to maintain low basal expression levels of LMP2 [21]. In addition, there is also some STAT1 phosphorylation (below detectable levels) in untreated cells that contributes to basal activity, as shown elegantly by knockin studies in mice [29]. We detected 2 STAT1 and 28 IRF1 binding sites in untreated cells, accounting for 2.2 and 14.3% of induced sites, respectively. Our data accords with another ChIP-chip analysis of STAT1 binding which reported that 6.5% of IFN γ -induced STAT1 sites in HeLa cells treated for 30 min with IFN γ (as opposed to 6 h in our case) are occupied in uninduced cells [22].



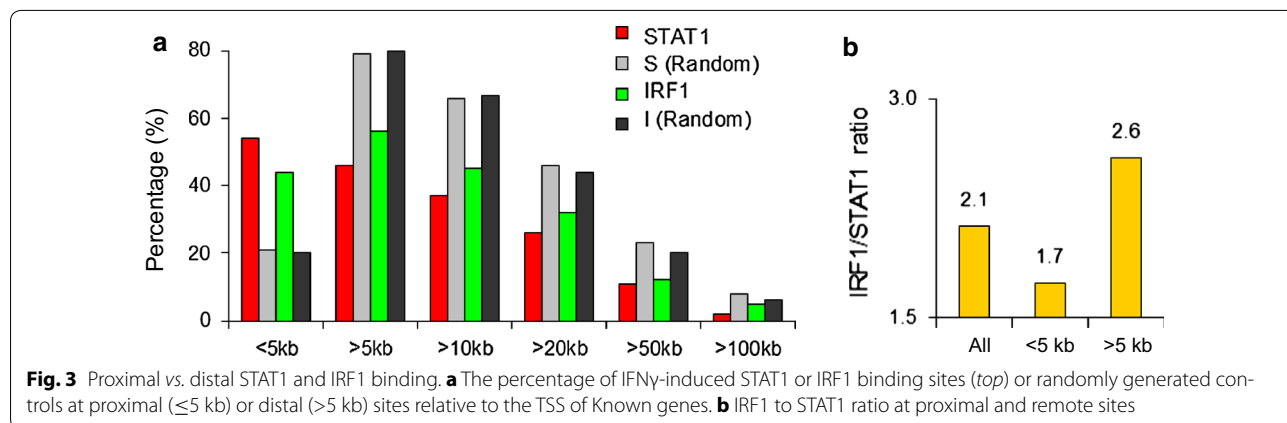
Further analysis suggests that basal TF binding detected here is physiologically relevant. Of the genes with basal STAT1 or IRF1 binding, we assessed 21 by microarray and/or RT-PCR and all were expressed in untreated cells (Additional file 1: Table S3). In contrast, of 26 randomly selected ISGs that lacked basal TF binding, only 13 were basally expressed. Indeed, constitutive expression of PSMB9 and TAP2 requires constitutive IRF1 binding [21, 30]. In addition, several loci with basal TF binding are in paralogous gene clusters suggesting conservation of high affinity binding sites during gene duplication (e.g. PSMB8 and PSMB9, GBP2 and GBP3, and IFIT1, IFIT2 and IFIT3). A high fraction (82%) of the 28 IRF1 basally occupied sites possessed IRF1 binding motifs. Thus, our data supports the notion that basal binding of STAT1 and IRF1 is physiologically relevant.

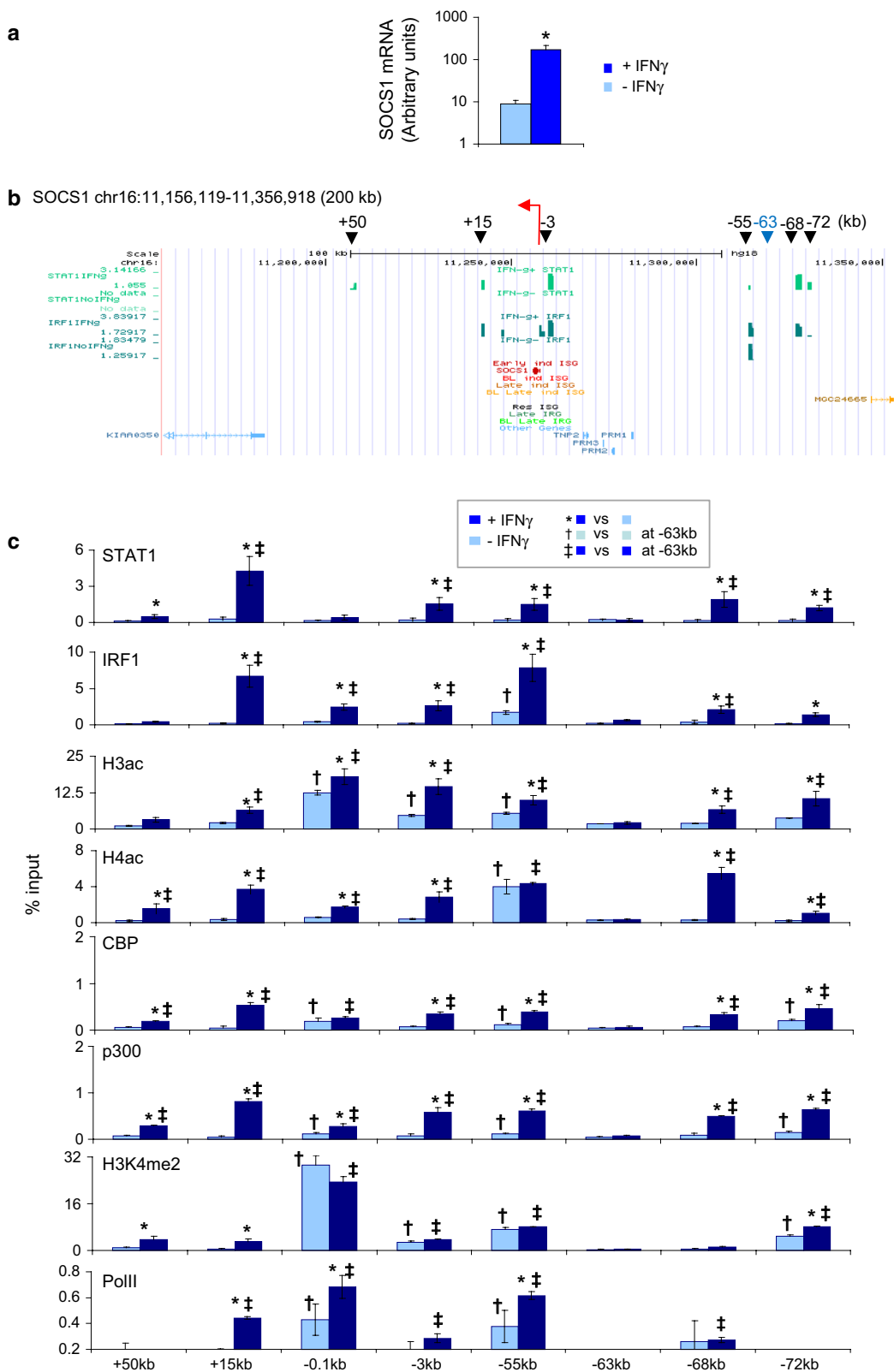
Remote IFN γ activated enhancers are common at ISGs

In IFN γ treated cells, 54% (50/92) of STAT1 and 44% (87/196) of IRF1 peaks were within 5 kb of the transcription start site (TSS) of all 394 Known Genes on the array (Fig. 3a; Additional file 1: Table S4). Adding other

databases, including predicted genes, raised the fraction to 64% for STAT1 and 57% for IRF1 (Additional file 2: Figure S2A). Of equal numbers of randomly generated sites, the proportion at <5 kb from gene starts was much lower (Fig. 3a; Additional file 2: Figure S2A). Thus STAT1 binding is slightly skewed to promoter proximal sites, while IRF1 binding is slightly biased toward remote sites (Fig. 3b).

Prior analysis of chromatin modification and looping at *CIITA*, and partial looping analysis at *1* locus support the idea that remote sites are functionally important [7, 8]. To further test this notion we performed additional assessment of *SOCS1*, a key negative regulator of IFN γ signaling that is responsive to IFNs and other immune signaling pathways [31, 32]. *SOCS1* responds to IFN γ in HeLa cells (Fig. 4a). ChIP-chip data exposed 6 IFN γ -induced STAT1 and/or IRF1 peaks \pm 100 kb of the *SOCS1* TSS (Fig. 4b). ChIP-qPCR analysis verified binding at the *SOCS1* promoter (*pSOCS1*; -0.1 kb), and at +50, +15, -3, -55, -68 and -72 kb (Fig. 4c). A negative region at -63 kb was also validated. In favor of functional relevance of proximal and remote sites, we detected constitutive histone H3 acetylation (H3ac) and/or H4ac at *pSOCS1* (-0.1 kb), -3 and -55 kb (Fig. 4c), and IFN γ induced acetylation at *pSOCS1* and the 6 remote sites but not at the irrelevant -63 kb site (Fig. 4c). These constitutive and inducible events paralleled recruitment of the HATs CBP and/or p300 (Fig. 4c). H3K4me2 also marks enhancers [33], and constitutive H3K4me2 was detected at *pSOCS1*, -3 kb, -55 kb, matching constitute histone acetylation, and also at the -72 kb enhancer (Fig. 4c), which contacts the promoter (see below). IFN γ treatment did not further increase methylation at these sites, but did induce H3K4me2 at +50 kb, +15 kb and -72 kb (Fig. 4c). Finally, we detected constitutive Pol II recruitment at *pSOCS1* and -55 kb but not at the other TF binding or negative control sites (Fig. 4c). After IFN γ treatment, Pol II recruitment increased at *pSOCS1*,





(See figure on previous page.)

Fig. 4 STAT1 and IRF1 binding at *SOCS1*. **a** RT-qPCR for *SOCS1* mRNA in HeLa cells treated with IFN γ for 0 or 6 h. Data are in arbitrary units relative to β -actin levels (log scale). **b** ChIP-chip maps of STAT1 and IRF1 binding across the *SOCS1* locus treated as in **a**. Black arrowheads indicate TF binding sites of interest, with distances from the TSS (red arrow) in kb. The TF-free -63 kb site (blue) is used as a negative control in **c**. **c** ChIP-qPCR analysis of the basal and IFN γ -induced histone modifications or recruitment of the indicated factors. Marks (*, †, ‡) show significant differences ($p < 0.05$, ANOVA followed by Fisher test) in the indicated comparisons (mean \pm SD, $n = 3$)

+15 kb and -55 kb (Fig. 4c). Association with the +15 kb element may reflect IFN γ -induced promoter looping (see below).

Chromosome conformation capture (3C) revealed both constitutive and IFN γ -induced contacts between the promoter and remote STAT1 and/or IRF1 sites at *CIITA* [7]. To examine looping at *SOCS1*, we studied six EcoRI (I–VI) or four NcoI (VII–X) fragments (Fig. 5a). Of a total of 22 possible interactions, we studied 4 previously ([8]; underlined in Fig. 5b) and assessed an additional 7 in this study. As expected, no interaction was observed between fragments containing the promoter and irrelevant sites at -63, -6, or +70 kb, either before or after cytokine exposure. However, between suspected functional elements, we detected a total of 3 loops of all 11 putative interactions in the basal state, and each of these loops was enhanced after IFN γ treatment and was accompanied by a new interaction between the +50 and -72 kb enhancers that lie 122 kb apart (Fig. 5b, c). Our data suggest that the *SOCS1* locus is basally present in a mega looping complex that becomes more compact and involves more inter-element interactions after IFN γ treatment. Together, the ChIP and 3C data show that STAT1 and IRF1 binding is linked to extensive chromatin modifications and looping.

Unusual IRF1 distribution at MHC loci

As noted earlier, IRF1 exceeded STAT1 sites by ~twofold, but this varied at some regions, most notably at the MHC class I locus where the ratio was 3.5:1 (56 IRF1:16 STAT1 sites; Additional file 1: Table S4). The ratio was particularly skewed at the extended (6:1) versus classic (2.9:1) MHC class I region. 26 of all MHC class I IRF1 sites were within 5 kb of Known Gene starts and 17 within 5 kb of pseudogenes (Additional file 1: Tables S4, S5), giving a total of 77% (43/56) promoter proximal sites, which is

higher than the 44% at all loci (Fig. 3a; Additional file 1: Table S4). However, whereas 66% (25/38) of IRF1 sites were promoter-proximal in the classical MHC class I region, this dropped to only 6% (1/18) at the extended MHC class I region, and was low even after including pseudogenes (4/18; Additional file 1: Tables S4, S5), leaving an unusually high fraction of remote IRF1 sites (78%). Thus, IRF1 seems to play a broader role than STAT1 at the MHC class I cluster, primarily at proximal elements in the classic region, but at remote elements in the extended region.

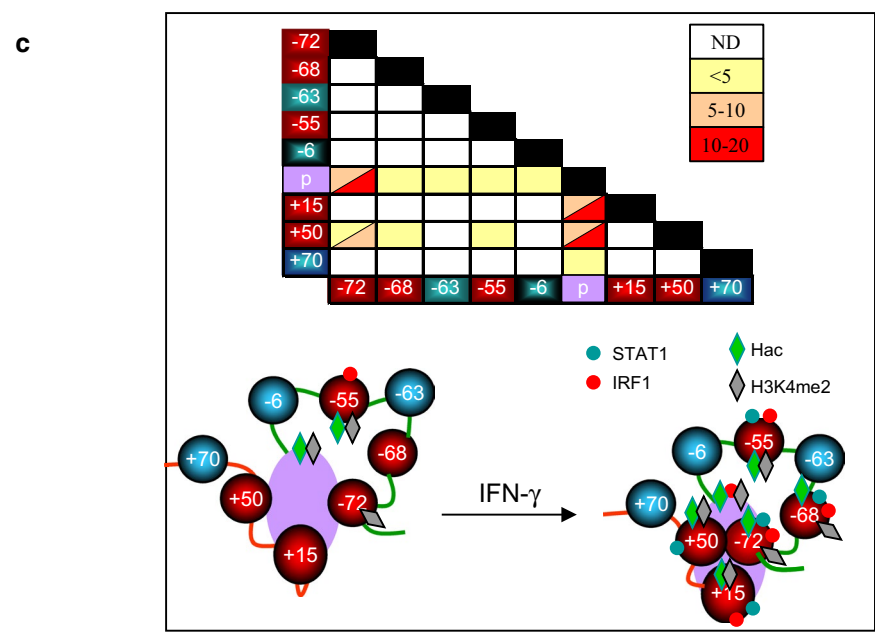
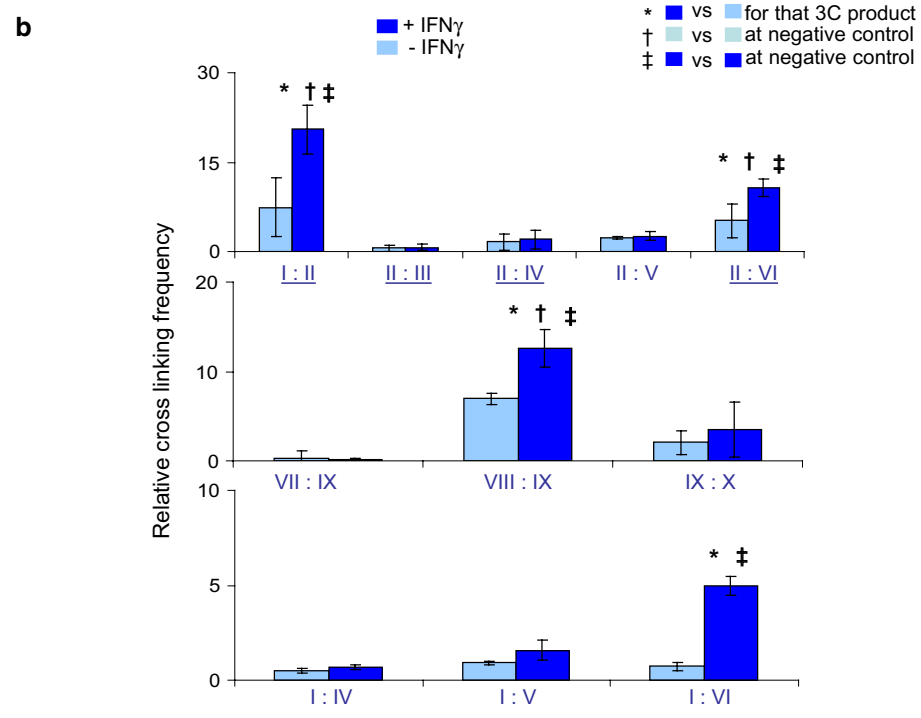
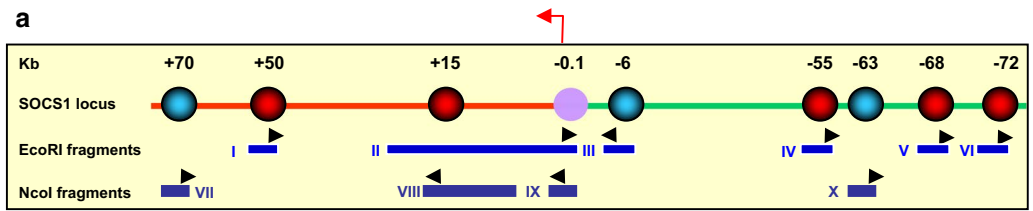
STAT1 and IRF1 induce *CIITA*, the master regulator of MHC class II expression (reviewed in [34]). The number of STAT1 and IRF1 sites was typically very low in the MHC class II region (Additional file 1: Table S4). Out of 13 MHC class II genes, 5 (DRB5, DQB1, DQB2, DQA2, and DOA) were resistant to IFN γ in HeLa cells, 5 (DOB, DRB1, DQA1, DPA1, DPB1) responded only after 24 h, a time of maximum production of *CIITA* [35], and 3 (DRA, DMB and DMA) were es-indISGs. With the exception of DOB, none of the resistant or late-induced genes exhibited STAT1 or IRF1 promoter binding. However, of the 3 es-indISGs, two had promoter proximal IRF1 binding while DMA had IRF1 binding fairly near (~8 kb) its promoter. Thus IRF1 may cooperate with *CIITA* at a subset of MHC class II promoters. Others reported *CIITA*-independent induction of MHC class II genes [36–39], which may, therefore, involve IRF1.

STAT1 and IRF1 binding is enriched at robustly induced ISGs

As discussed, ISGs fell into 8 classes depending on whether IFN γ caused induction, no effect (resistant ISGs in HeLa cells), or repression, and whether induction/repression were early or late, and strong or weak (Fig. 1b). We plotted the distribution of STAT1 and IRF1

(See figure on next page.)

Fig. 5 Basal and IFN γ -induced looping at *SOCS1*. **a** A schematic view of the *SOCS1* locus. Circles indicate the *SOCS1* promoter (purple), putative remote enhancers (red), and negative control sites (blue), with distances from the TSS (red arrow) indicated above in kb, while fragments used in 3C assays with primers (black arrowheads) are shown below. **b** Cross linking frequencies between the promoter and remote sites across the *SOCS1* locus. Quantitative 3C was performed with chromatin from HeLa cells left untreated or exposed to IFN γ for 6 h. Bar graphs show the crosslinking frequency of a selected number of interactions. Underlined interactions were published previously [8]. Marked interactions (*, †, ‡) are significantly different at the indicated comparisons ($p < 0.05$, ANOVA followed by Fisher test, mean \pm SD, $n = 3$). **c** Summary of looping events. Interacting sites and DNA strands are colored as in **a**. STAT1/IRF1 (green/red dots) and Hac/H3K4me2 (green/gray diamonds; data from Fig. 6c) are also depicted



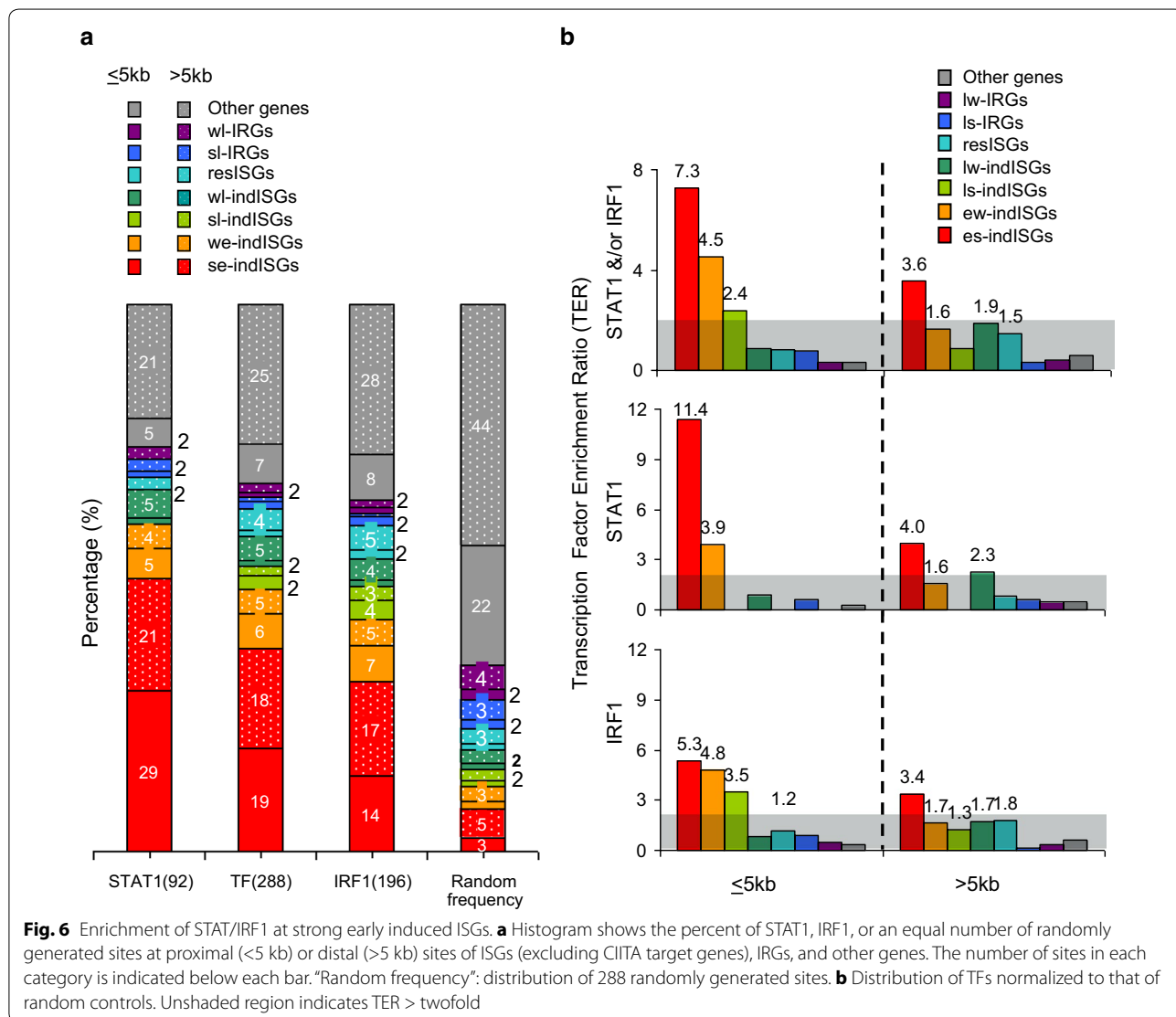
binding sites relative to all 8 gene classes. Binding sites were assigned to the nearest gene class, designated as proximal or distal when ≤ 5 or >5 kb from the TSS, respectively, and were compared to 288 randomly chosen sites equaling number of STAT1 + IRF1 sites (Fig. 6a). We also calculated the TF enrichment ratio (TER) in which the % distribution of TFs at proximal and distal locations was normalized to the % distribution of random sites (Fig. 6b). A binding frequency twice that of random sites (TER = 2) was assigned as an arbitrary minimum threshold.

STAT1 and IRF1 binding sites were most highly associated with robustly induced IFN γ targets (es-indISGs; Fig. 6). This applied when STAT1 or IRF1 were considered together, separately, and at proximal or remote locations (Fig. 6b). Consistent with this finding, weakly induced genes (ew-indISGs) had fewer binding events

and lower TERs (Fig. 6). Of 236 Other genes (never classified as an ISG in any study), a total of only 17 had 9 STAT1 and 16 IRF1 proximal peaks, mostly (13/17) located at the MHC and RT-qPCR confirmed no induction at 10/10 of these genes (Additional file 1: Table S6). IFN γ enhancers loop over large distances at *CIITA* [7] and *SOCS1* (Fig. 5), so proximal and distal enhancers nearest to Other Genes may target neighboring ISGs. In summary, the data indicate a clear bias of STAT1 and IRF1 binding at rapidly and robustly induced ISGs, but not other gene classes.

Isolated or dual STAT1 and IRF1 recruitment is directed by binding motifs

Next we compared the fraction of isolated or dual STAT1/IRF1 binding events. Of a total of 230 discrete



TF binding regions, 16% (36/230) exhibited STAT1 binding alone (isolated STAT1), of which almost half (17/36) were proximal; 61% (140/230) exhibited only IRF1 binding (isolated IRF1), of which 42% (59/140) were proximal; and 23% (54/230) showed overlap (dual STAT1/IRF1), of which slightly more than half (31/54) were proximal (Additional file 1: Table S4). Randomly generated sites showed negligible overlap (Additional file 2: Figure S2B), but dual STAT1/IRF1 binding represented more than half (54/92; 59%) of all STAT1 sites and about a quarter (54/196; 28%) of IRF1 peaks (Fig. 7a). Fewer overlapping IRF1 peaks reflect their twofold excess relative to STAT1 peaks. Thus, STAT1 preferentially binds with IRF1 at IFN γ enhancers, whereas most IRF1 sites are not colocalized with STAT1.

JASPER analysis of IRF1 and STAT1 peak regions revealed that the cognate binding motif was observed at a statistically significant level relative to equal numbers of random peaks (Fig. 7b). 60% of isolated STAT1 peaks had a STAT1 motif, and only 30% had an IRF1 motif, while 70% of isolated IRF1 peaks possessed an IRF1 motif, but only 20% had a STAT1 motif. A strong correlation existed between STAT1/IRF1 binding and the presence of the corresponding motifs (Fig. 7c). Indeed 40% of dual STAT1/IRF1 sites had both binding motifs, whereas there were none at equal numbers of randomly generated sites (Fig. 7b). Dual sites which have only a STAT1 or IRF1 binding motif may reflect protein–protein interaction or DNA looping as seen at the *SOCS1* and *CIITA* loci (Fig. 4c) [7, 8]. In summary, DNA sequence directs isolated or dual STAT1/IRF1 binding in IFN γ treated cells.

Dual STAT1 and IRF1 targeted enhancers distinguish responsive from resistant ISGs

Comparing inducible ISGs in our array study with ~all known ISGs in a large database (Additional file 1: Table S2) revealed resistant ISGs (res-ISGs) in HeLa cells (Fig. 1b). There were far fewer STAT1/IRF1 binding events at res-ISGs vs ind-ISGs, and the TER (ratio of actual TF binding to random sites) at res-ISGs was low, and similar to that at other genes (Fig. 6). There was near ubiquitous association of both STAT1 and IRF1 at es-indISG promoters, but they were virtually absent at res-ISG promoters (Fig. 6). To quantify the types of TF binding events (isolated, dual, etc.), we plotted the frequency of genes with at least one binding event within or beyond 5 kb (Fig. 8b), and the density of each type of binding event per gene (Fig. 8c). Isolated TF binding did not discriminate the two gene classes, whereas there was significantly more dual STAT1 and IRF1 binding at esISGs, at both proximal and distal sites (Fig. 8b, c). Thus, cooperation between STAT1 and IRF1 plays a central role in mediating IFN γ responsiveness.

Degree of TF binding and responsiveness in HeLa predicts ISG responsiveness in other cell types

Many studies have analyzed IFN-gene responsiveness, but a comprehensive analysis of which ISGs show broad or cell-type specific expression and, more importantly, the mechanism underlying such variability, has not been attempted. To assess variability in ISG induction, we compiled expression data on ISGs from 7 different human cell lines or primary cells, including 5 listed in Additional file 1: Table S2, plus HeLa cells (this work) and BRG1-reconstituted SW13 cells [13]. Across all 7 cell lines there were a total of 312 ISGs, the majority (61%) were exclusively induced in only one cell type, 28% were induced in 2–4 cell types, and 11% were induced in most (5–7) cell types (Fig. 9a; Additional file 1: Table S8). Only 9 genes were induced in every context and these included STAT1 and IRF1, in line with their apical role in IFN γ signaling.

We assessed the relationship between broad responsiveness, degree of induction, and STAT1/IRF1 binding. HeLa ChIP-chip data provided STAT1 and IRF1 binding information for 24 es-indISGs present in all 7 expression array datasets. Of these, 3/24 were induced exclusively in HeLa, 10/24 were induced in 2–4 lines and 11/24 were induced in 5–7 lines (Fig. 9b). Of note, genes induced exclusively in HeLa were up-regulated to a much lower extent than ubiquitously IFN γ -responsive targets (Fig. 9c). Greater induction of ubiquitously responsive loci was paralleled by a higher density of TF binding at promoter proximal sites (Fig. 9d). Thus, the level of induction is linked to the degree of STAT1 and IRF1 recruitment, and there is an unexpected link between the strength of ISG induction in one context (HeLa in this case) and competency to respond to IFN γ in other contexts.

SNPs modulate STAT1 and IRF1 binding in vitro

Defects in IFN γ signaling are linked to a wide range of disorders [40–44]. Several studies focused on the association between genetic variants and the risk of IFN γ related disorders, but at gene promoters or coding regions of ISGs rather than IFN γ responsive enhancers. Within the 16 Mb of DNA around ISGs studied here, there are a total of 7.1×10^5 dbSNPs [hg19; SNPs (141)]. Of these, 6648 dbSNPs lay within the 230 STAT1/IRF1 peaks. Only 7 of these 6648 dbSNPs were listed on the GWAS database. GWAS SNPs do not define all disease associated SNPs (DA-SNPs) because GWAS genotyping arrays provide low genomic coverage [45] and therefore the 6648 dbSNPs may encompass other DA-SNPs not mapped yet. None of the 7 DA-SNPs (GWAS database) overlapped with a STAT1/IRF1 motif, but 80 of the 6648 dbSNPs overlapped with 27 STAT1 and 47 IRF1 motifs (Additional file 1: Table S9).

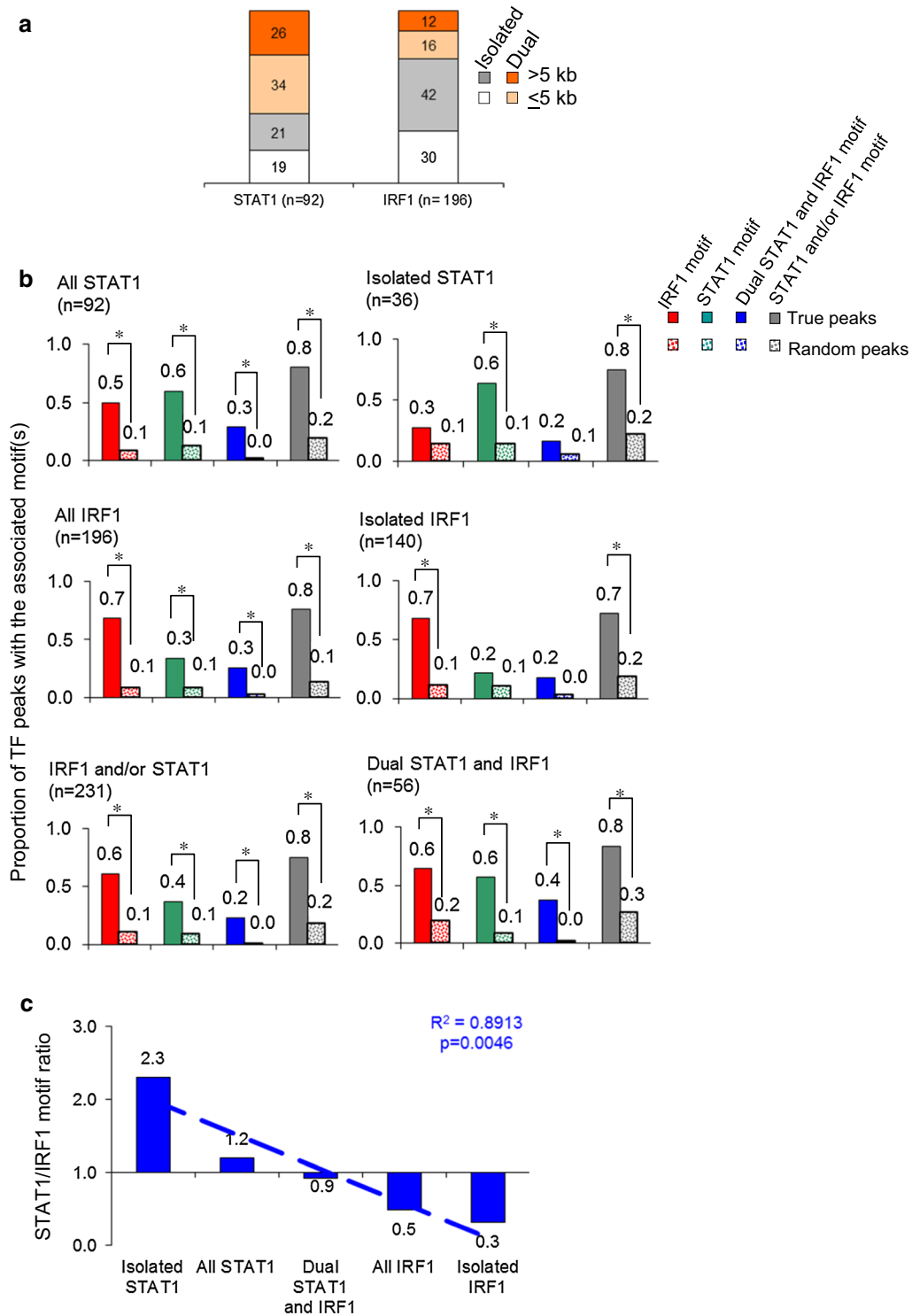


Fig. 7 STAT1 and IRF1 binding correlates with binding motifs. **a** Percent distribution of isolated STAT1 or IRF1 or dual STAT1 + IRF1 binding at proximal (≤ 5 kb) or remote (> 5 kb) sites of Known gene promoters. **b** TF binding sites were classified into 6 subclasses, then mapped motifs using CisGenome’s “Known Motif Mapping” program (see “Methods” section for details). Sets of equal numbers of randomly generated “peaks” were used to define the background occurrence of STAT1 and IRF1 motifs. Asterisk indicates significant difference between true and random peaks ($p < 0.00005$, two-sided probability test in R). **c** Ratio of STAT1/IRF1 motifs at different categories of peaks

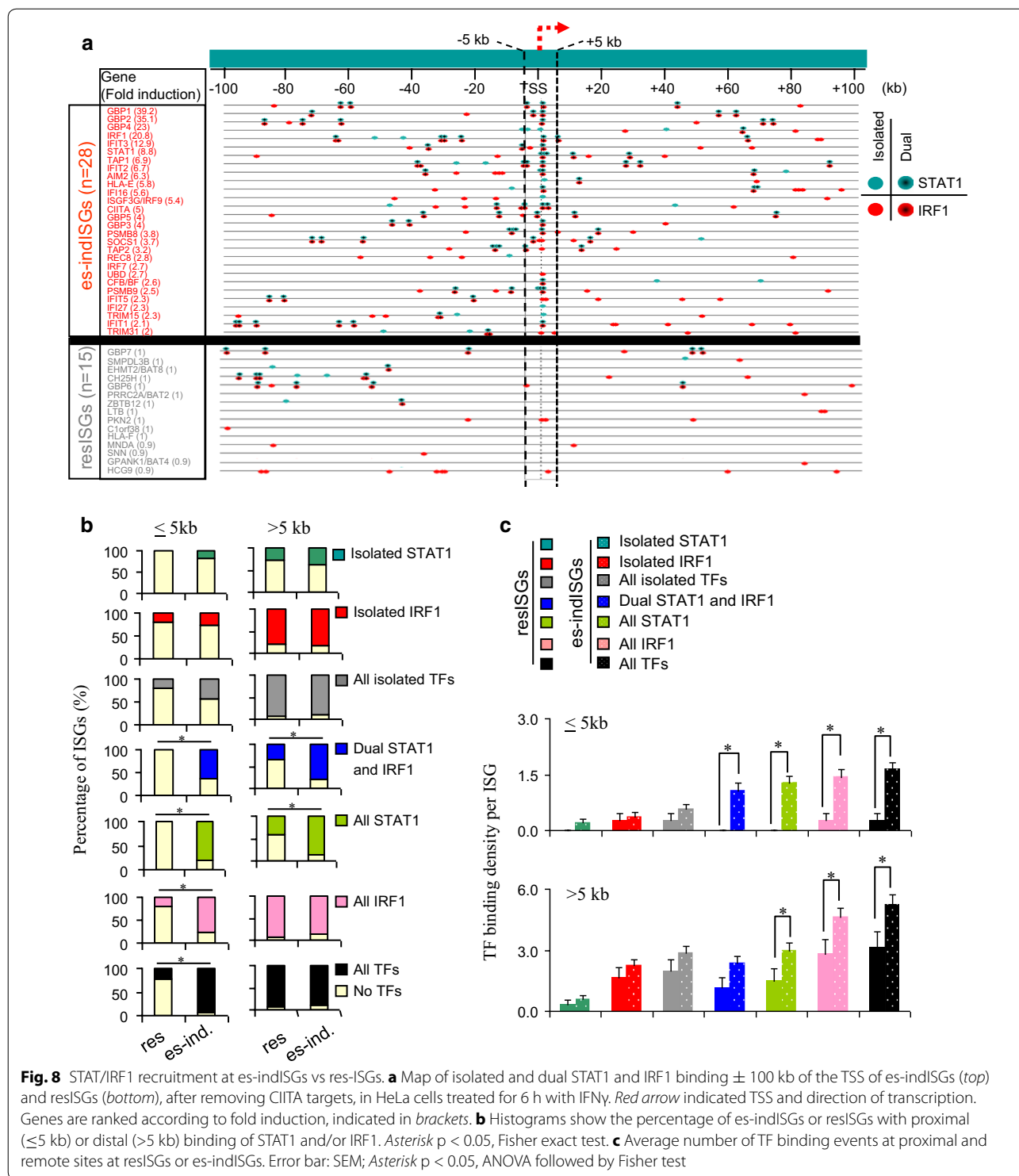


Fig. 8 STAT/IRF1 recruitment at es-indISGs vs res-ISGs. **a** Map of isolated and dual STAT1 and IRF1 binding \pm 100 kb of the TSS of es-indISGs (top) and resISGs (bottom), after removing CIITA targets, in HeLa cells treated for 6 h with IFN γ . Red arrow indicated TSS and direction of transcription. Genes are ranked according to fold induction, indicated in brackets. **b** Histograms show the percentage of es-indISGs or resISGs with proximal (\leq 5 kb) or distal ($>$ 5 kb) binding of STAT1 and/or IRF1. Asterisk $p < 0.05$, Fisher exact test. **c** Average number of TF binding events at proximal and remote sites at resISGs or es-indISGs. Error bar: SEM; Asterisk $p < 0.05$, ANOVA followed by Fisher test

We studied which of these 80 SNPs affect STAT1/IRF1 binding. First, we utilized the CisGenome “Known Motif Mapping” program to predict which of the variants may modulate STAT1/IRF1 binding motifs (see “Methods” section). CisGenome compares the position

weight matrix (PWM) in the JASPAR CORE database and creates likelihood scores for the reference or variant allele. We calculated the fold change in likelihood scores (variant/reference allele) to assess the predicted relative effect. At a cutoff of 1.5-fold, the variant alleles of 34/80

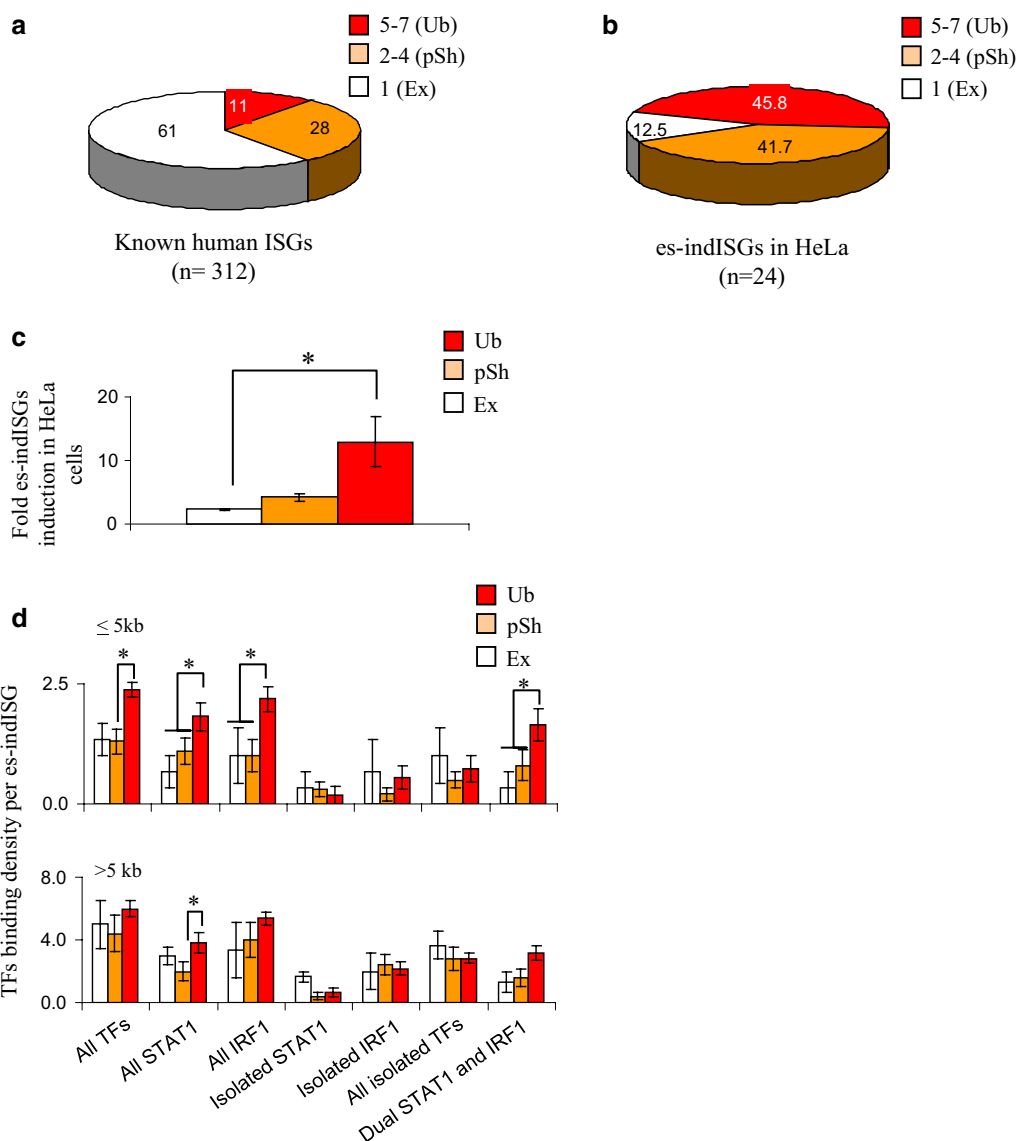


Fig. 9 Link between ISG responsiveness in HeLa cells, responsiveness in other cell types, and STAT1/IRF1 binding. **a** Percentage of ubiquitous (Ub), partially shared (pSh), or exclusive (Ex) human ISGs based on their responsiveness to IFN γ in the indicated number of cell lines. **b** Percentage of HeLa es-indISGs which respond in only HeLa or in more cell types (as in **a**). For full lists of ISGs and es-indISGs see Additional file 1: Tables S7, S8. **c** Level to which Ub, pSh or Ex es-indISGs are induced in HeLa cells. **d** Average number of TF binding at promoter (≤ 5 kb) and remote (> 5 kb) sites of the indicated types of es-indISGs. Error bar indicates SEM; Asterisk $p < 0.05$, ANOVA followed by Fisher test

dbSNPs were predicted to modulate the binding affinity of 24 IRF1 motifs and 10 STAT1 motifs (Additional file 1: Table S9).

To test these predictions in vitro, we developed an ELISA-based DNA affinity assay (see “Methods” section). Canonical STAT1 or IRF1 motif-containing biotinylated 33-mers were immobilized on streptavidin-coated 96-well plates. Cell lysates from HeLa cells exposed to IFN γ for 6 h were mixed with either no or various amounts of Wt (positive control), mutated (negative control), or dbSNP (test) competitor probes, then added to

the immobilized biotinylated probe, and the amount of bound TF determined using anti-STAT1 or anti-IRF1 antibody. We tested 4 or 1 SNPs affecting IRF1 or STAT1 sites, respectively (Fig. 10; Additional file 1: Tables S9, S10). Wt IRF1 and STAT1 probes exhibited strong binding with low IC_{50} s of 9.6 ± 1.5 or 4.2 ± 0.9 pmol/well, respectively, whereas control mutated probes had minimal/no effect (Fig. 10; Additional file 1: Table S10). 3/6 of the IRF1 SNPs decreased affinity (rs365393, rs9262216, rs34494346) and 1/6 created a strong IRF1 site (rs9260102) (Fig. 10a; Additional file 1: Table S9). The

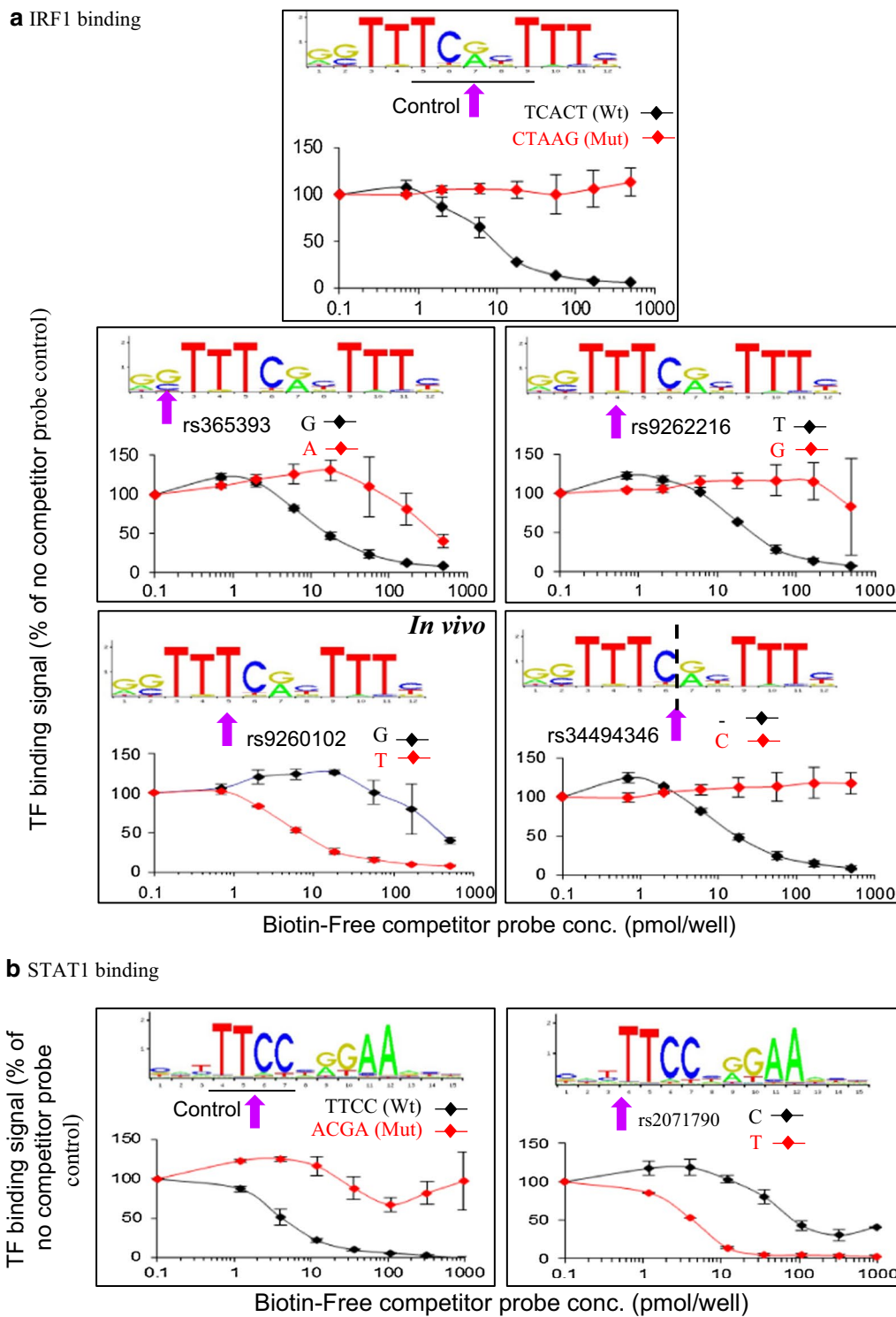


Fig. 10 SNPs modulate STAT1 and IRF1 binding in vitro. **a** IRF1, and: **b** STAT1 binding assays. Graphs show STAT1 and IRF1 binding signal to immobilized probes in the presence of different concentrations of competitor probes with either the variant or reference allele. 100% binding is that obtained in the absence of competitor. Arrows highlight the affected base (or 4 bases in the control mutated probe). As indicated, rs9260102 was also assessed in vivo (Fig. 11)

single STAT1 SNP that we tested created a putative binding site, and indeed the T allele of rs2071790 showed high affinity binding (Fig. 10b; Additional file 1: Table S10). Our CHIP-chip data indicated that this SNP lies within an isolated remote IRF1 peak, suggesting that the T allele would convert this regulatory element to a dual STAT1/IRF1 enhancer. In summary, these data show close concordance between the predicted and actual effects of SNPs on STAT1 and IRF1 binding. Thus, it is likely that most of the 34 predicted functional SNPs do in fact alter binding.

rs9260102 affects IRF1 binding in vivo

Next we asked if the T allele of rs9260102, which creates an IRF1 site in vitro (Fig. 10a), has this effect in vivo. This SNP lies ~1 kb upstream of the HLA-A locus, within an IFN γ -responsive IRF1 CHIP-chip peak in HeLa cells

(Fig. 11a). To test whether it affects IRF1 binding in vivo we employed the EBV-transformed lymphoblastic cell line GM18857, which is heterozygous for rs9260102 (G/T), implying that IRF1 should only bind to one (the T) allele. Treatment with IFN γ for 6 h induced a 1.8-fold increase in the total IRF1 CHIP-qPCR signal (Fig. 11b). Snapshot sequencing revealed that this IFN γ -dependent increase was due solely to elevated binding to the T allele (Fig. 11c). Thus, in silico prediction, an in vitro binding assay, and in vivo allele specific ChIP all show that the G to T switch creates an IRF1 binding site (Fig. 10a; Additional file 1: Table S10).

Discussion

STAT1 and IRF1 drive the induction of IFN induced genes, but the extent to which they act collectively is unclear. We report that most STAT1 binding (60%)

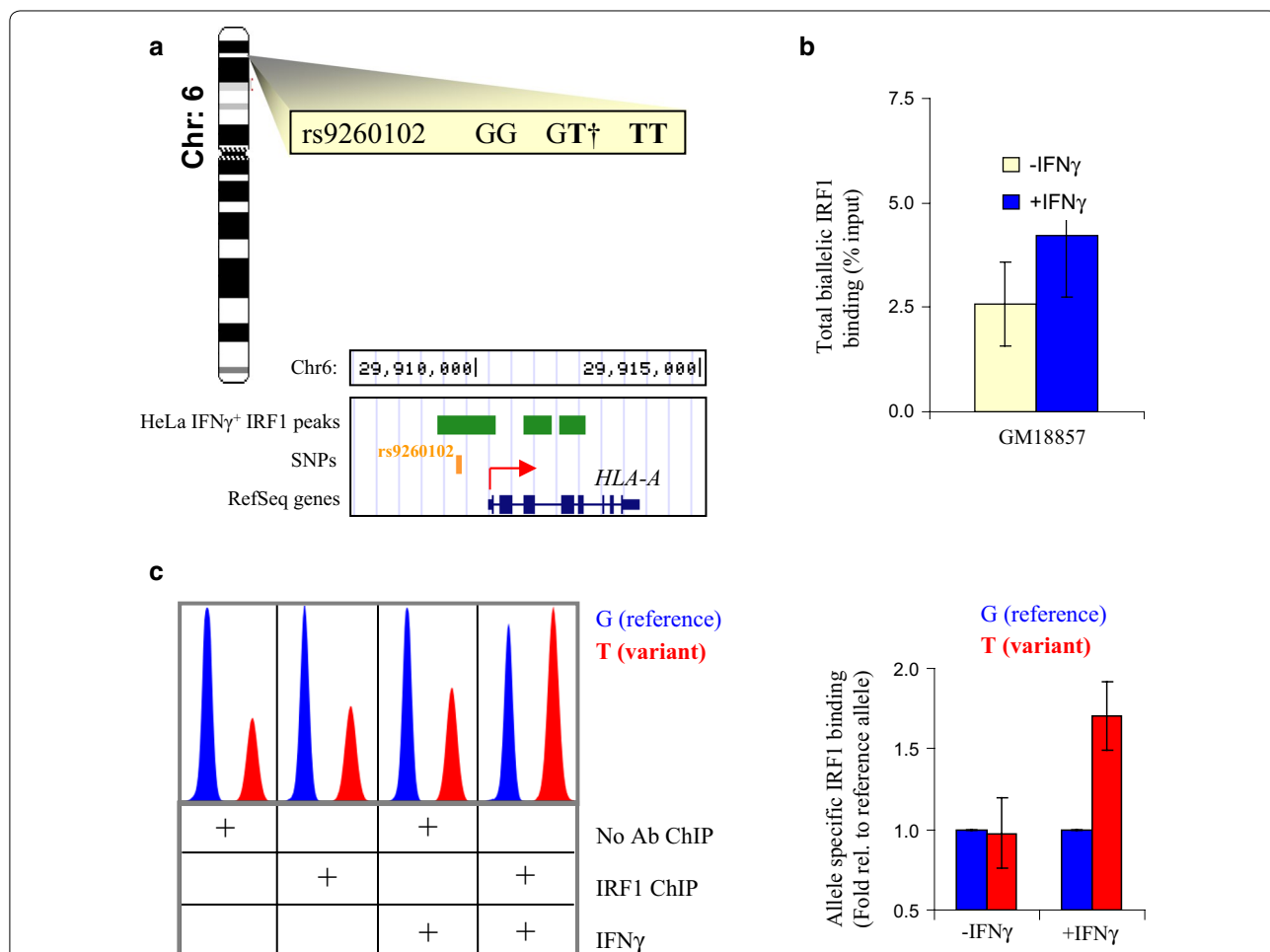


Fig. 11 rs9260102 modulates IRF1 binding in vivo. **a** Chromosomal location of rs9260102 and the alleles (strong IRF1 binding in *bold*), and a genome browser view of the SNP, which lies upstream of *HLA-A* and within an IFN γ -induced IRF1 Chip-chip peak in HeLa cells. **b** ChIP-qPCR of basal and IFN γ -induced IRF1 recruitment at rs9260102 in GM18857 EBV transformed lymphocytes. **c** Electropherogram on left shows snapshot sequencing of ChIP DNA, with peak quantification plotted on the right (mean \pm range, n = 2)

occurs together with IRF1, but most IRF1 binding (72%) is isolated (Fig. 7a). Binding occurs where there are cognate binding motifs (Fig. 7), suggesting that most ChIP signals reflect direct recruitment. Both proximal and remote STAT1 and IRF1 binding is observed at robustly induced ISGs, but not at other loci (Fig. 6). In line with the importance of TF occupancy for responsiveness [46], every responsive locus exhibits a mixture of STAT1 and IRF1 bound enhancers (Fig. 8a). Moreover, dual bound enhancers distinguish induced vs resistant ISGs, whereas single bound enhancers are found with similar frequency at responsive or non-responsive ISGs (Fig. 8). This is not to say, however, that single bound enhancers are irrelevant. For example, while multiple remote *SOCS1* enhancers recruit both TFs, the +50 kb element or promoter are targeted only by STAT1 or IRF1, respectively, yet both are involved in 3D looping (Figs. 4, 5). Similarly, while dual STAT1/IRF1 binding occurs at the active *CIITA* promoter, the -50 kb and +59 kb enhancers recruit only STAT1 or IRF1, respectively, yet contribute to 3D looping and are essential for responsiveness [7]. Indeed, all the responsive genes we surveyed exhibit a mix of STAT1-only, IRF1-only, and STAT1/IRF1 dual enhancers (Fig. 8). Together, these results suggest that IFN γ -responsiveness requires cooperation between enhancers that bind both or either TF, but that STAT1- or IRF1-only enhancers are insufficient for gene induction. Irrespective, it is clear that responsive ISGs integrate information from both STAT1 and IRF1.

Previously, we showed that there is a pre-existing 3D structure at the silent *CIITA* locus, generated through looping between enhancers that subsequently recruit STAT1 and IRF1 upon IFN γ treatment [7]. This was true even in the absence of BRG1, a chromatin remodeling enzyme that is critical to allow stable TF recruitment and thus IFN γ -responsiveness. Subsequent genome-wide analyses indicate that enhancer looping in the poised but silent state is common at inducible loci [47]. We observed the same phenomenon at the IFN γ responsive *SOCS1* locus (Fig. 5). Potentially, these contacts are mediated by pioneer factors that mark responsive enhancers, but their identity at ISGs is unknown. The data here and other studies show that STAT1 and IRF1 can bind some sites in the basal state [21, 28], so in theory, low/unstable binding (undetectable by ChIP) could poise ISG enhancers. It would thus be interesting to perform looping studies at ISGs in STAT1/IRF1 deficient cells. It is of note that the degree to which ISGs were induced in HeLa cells predicted whether they were likely to respond to IFN γ in other cells (Fig. 9). Thus, the chromatin at these genes is accessible in many contexts. The factors that mediate this broad poised, open state may also initiate the basal looping at ISGs.

Over 90% of the disease markers identified in GWAS studies lie within the non-protein-coding regions of the genome [48]. These markers correlate with gene expression [49–52], and lie within gene regulatory regions [53–56]. There is thus considerable interest in identifying SNPs that influence TF binding and, therefore, gene regulation. We identified 80 SNPs within STAT1 or IRF1 motifs, and in silico assessment predicted that 34 may alter binding. In vitro quantification confirmed these predictions in 5/5 cases, arguing that most of/all the other predictions are accurate. The availability of a cell line heterozygous for one such SNP allowed us to test whether the prediction held up in vivo. Indeed, the T allele of rs9260102, which lies just upstream of the HLA-A locus, bound IRF1 whereas the G allele did not, as observed in silico and in vitro. These data serve as proof of principle that in silico prediction is a reliable tool to anticipate the effect of SNPs on STAT1 and IRF1 binding.

Conclusions

This study provides strong evidence for widespread cooperation between STAT1 and IRF1 at ISGs, and suggests that in silico predictions reliably predict the effect of nucleotide variants on binding in vivo.

Methods

Custom oligonucleotide ChIP Tiling array design

A custom oligonucleotide tiling array was designed to cover 11 genomic regions spanning a total of 16 Mb of human genomic DNA in 8 chromosomes (Additional file 1: Table S1). Regions covered from 1 to 5 Mb genomic sequences. Arrays consisted of 50 mers, in quadruplicate, with median probe spacing of 80 bp within non-repetitive DNA regions.

ChIP on tiled genome arrays (ChIP-chip) and ChIP-quantitative PCR

Details of primers and antibodies used in ChIP assays are in Additional file 1: Tables S11, S12. HeLa-ini1-11 cells (HeLa), were grown as described [12]. Cells were left untreated or exposed to 300 units/ml of human IFN- γ for 6 h (PHC4834, BioSource International, Camarillo, CA, USA). Crosslinked chromatin was sonicated to an average size of about 500 base pairs and was incubated with STAT1 or IRF1 antibody. Bound fragments were purified by ChIP and amplified by ligation-mediated PCR, as described [7], then labeled and hybridized to the arrays. Hybridization intensities were normalized to internal standards and values from quadruplicate spots were averaged. Significantly different intensities between ChIP DNA and input DNA samples in three biological replicates ($p < 0.0001$) were determined with the Wilcoxon rank-sum test. Peaks representing significantly enriched

DNA regions ($p < 0.0001$) where the ratio of ChIP to input DNA was 1.5-fold or more were visualized with the University of California at Santa Cruz Human (*Homo sapiens*) Genome Browser (Phast-Cons) and are plotted on a log₂ scale. Peaks in a sliding window of 500 base pairs were merged with an in-house Perl script pipeline. ChIP—quantitative PCR was done as described [7], and in all cases, the low background signal obtained with a no-antibody control was subtracted.

Custom oligonucleotide ChIP tiling array data analysis

Raw intensities from three independent biological replicates, quality assessed by Nimbelgen SignalMap software, were quantile normalized [57], and averaged for each quadruplicate 50 mer. We developed a Wilcoxon Rank Sum test [58] based software to studying the difference between the intensities of the ChIP signal compared to the input DNA signal for each probe within a 500 bp sliding window. Genomic positions with statistically higher intensities (>1.5 -fold, $p < 10^{-4}$) from input DNA were merged to form a peak. ChIP-chip data were imported into UCSC genome browser (assembly hg17, NCBI build 35) as two sets of separate tracks for each antibody before and 6 h after IFN γ treatment (<http://research.lunenfeld.ca/IFN\gamma>).

STAT1 and IRF1 motif analysis

We mapped STAT1 and IRF1 consensus motifs to the STAT1 and IRF1 ChIP-chip binding regions by using CisGenome “Known Motif Mapping” program. Motif occurrences were determined by using position frequency matrices (PFMs) of STAT1 (ID: MA0137.2) and IRF1 (ID: MA0050.1) from the JASPAR CORE database. The PFMs were converted to pseudo-count matrix for CisGenome’s input. A motif mapping location is selected by the cut-off of a likelihood ratio (LR) > 500 . The LR is determined by comparing the motif’s PFM with a background model estimated from input ChIP-chip regions in the 3rd order. Seven sets of ChIP-chip peak regions were mapped and compared with background control regions: STAT1 peaks (92), IRF1 peaks (196), merged STAT1 and/or IRF1 peaks (231), dual STAT1 and IRF1 peaks (56), STAT1 peaks isolated from IRF1 peaks (isolated-STAT1, 56), IRF1 peaks isolated from STAT1 peaks (isolated-IRF1, 140), and basal IRF1 peaks. For each set of peaks, the same number and size of control background regions were randomly sampled from blank regions without any ChIP-chip bindings following the same frequency distribution as the real binding peaks within each cluster segments on the chromosome of ChIP-chip data. The frequencies of regions mapped with motifs were compared between ChIP-chip peaks and random control sites by using the two-sided probability test in R for each paired set of peaks.

RNA extraction, expression microarray analysis, and Reverse transcriptase-qPCR

RNA extraction and reverse transcription were done from HeLa cells left untreated or at 6, 24 or 48 h after IFN γ treatment as described previously [12]. RNA quality was checked using both Nanodrop (Thermo Fischer Scientific; 260/280 ratio was ≥ 1.8) and Bioanalyzer (Agilent Inc.; RNA Integrity Number, RIN, ≥ 9.4 , range 9.4–9.9). RNA samples were converted to cDNA, followed by a second strand synthesis, and cRNA was prepared using the Ambion kit (Applied Biosystems). The cRNA was column purified and quality was checked using Bioanalyzer (Agilent Inc.). A total of 1.5 μ g of cRNA was hybridized to human whole-genome expression arrays (HumanRef-6 Expression BeadChip, Illumina, Inc.) using standard Illumina protocols. Slides were scanned on an Illumina Beadstation and analyzed using BeadStudio (Illumina, Inc). Genes induced by \geq twofold compared to controls and that achieved a differential score of ≥ 13 were classified as strongly induced ISGs. ISGs which achieved a differential score of ≥ 13 but fold induction less than 2 were considered weakly induced. Genes reduced by \geq twofold compared to control and achieved a differential score of ≤ -13 were considered strongly reduced. Genes that had a differential score of ≤ -13 but the fold reduction was less than 2 were considered weakly reduced. Three biological replicates were included for each treatment group.

RT-qPCR was performed much as described [59]. Briefly, RNA was extracted from HeLa cells left untreated or at 6, 24 or 48 h after IFN γ treatment using Trizol (Invitrogen), and quality assessed by RIN and OD260/280 as above. cDNA was prepared from 1 mg RNA using random primers and SuperScript RT (Invitrogen). Amplification of cDNA was performed using gene specific primer pairs and SYBER Green Mix (ABI). PCR was ran on Applied Biosystems PRISM 7900HT. Primers were designed in the coding region of each gene (Additional file 1: Table S12). Human genomic DNA was used to prepare calibrators for the quantification of cDNAs. Dissociation curves were inspected to ensure a single product and all PCR products were also tested on a gel to confirm amplification specificity. In addition, no template controls (NTC) were included to ensure the absence of DNA contamination. Gene expression was normalized to multiple house-keeping/reference genes to control for the total amount of RNA. All experiments were done in triplicate.

Chromosome conformation capture (3C)

The 3C assay was conducted as described [7, 8]. Primer sequences are provided in Additional file 1: Table S12.

Assessment of TF binding distribution around different classes of ISGs

We compared the distribution of TFBS in the vicinity of es-indISGs and resISGs in STAT1 peaks, IRF1 peaks, and merged STAT1 and IRF1 peaks. We first aligned the TFBS within a range of 400 kb region around the TSS of each gene in a 1 kb resolution, which means that we divided each region into 1 kb windows with the window 0 centered at the TSS and others line up to the 200 kb end upstream and 200 kb end downstream, and then scored the frequency of TFBS at each window as the number of peaks whose center was within the window. If 400 kb extended beyond the ChIP-chip segments, the binding frequencies along the truncated regions were regarded as missing data. Then we plotted the average binding frequencies per 1 kb window versus the relative distance of each to the TSS. Missing values were discarded for averaging the frequencies.

Defining STAT1 and IRF1 functional SNPs

First, we queried dbSNPs located within the 230 ChIP-chip peaks (UCSC, Build hg19; Track, All SNPs(141); Table, snp141). We defined a total of 6648 dbSNPs. Next we defined SNPs that overlap with STAT1 or IRF1 binding motifs within the 230 ChIP-chip peaks. Then we selected a region of ± 50 bp around the SNPs that overlapped with STAT1/IRF1 binding motifs and recovered the DNA sequence of these regions using CisGenome. Then we computationally evaluated the binding affinity of the reference or variant sequence using the likelihood scores obtained from the CisGenome “known motif mapping” program with the sequences as input to map the STAT1 and IRF1 motif matrix. In some cases the introduction of the variant SNP renders the motif unidentifiable and in this case the sequence of the motif was indicated as “NULL” and the likelihood score was considered as zero (Additional file 1: Table S9). The cutoff value of affinity change was set at 1.5-fold.

ELISA-based DNA binding affinity assay and ChIP coupled with DNA sequencing

We designed 33-mers with either the reference or variant alleles (Additional file 1: Table S13). Control probes with wild type or dead mutant STAT1 or IRF1 motifs were also included. Probes were ordered biotinylated or biotin-free (competitors). Two pmol of biotinylated probes were immobilized per well of 96-well streptavidin-coated plates. Cell lysates were incubated with different concentrations of the competitor probes (probe-lysate mix) at 4 °C for 3 h to allow STAT1 or IRF1 binding. The probe-lysate mix was then added to streptavidin-coated plates with immobilized biotin probes and incubated overnight at 4 °C. To quantify bound TFs, wells were

washed and probed with STAT1 or IRF1 primary antibodies, followed by IR-800 conjugated secondary antibodies. Excess antibodies were washed thoroughly and plates were scanned and quantified using Odyssey Infra-red imaging system (LICOR). Signal from no-competitor well is considered as 100% and the % antibody signal was plotted against competitor probe concentration. IC50 values were calculated using Graphpad PRISM 5.2.

For in vivo studies, EBV-transformed lymphoblastic GM18857 cells, cultured as recommended by the supplier (Coriell Biorepositories), were treated with IFN γ for 6 h, fixed and harvested for ChIP analysis. Chromatin was immunoprecipitated using IRF1 antibody and isolated DNA was sequenced using Snapshot sequencing.

Additional files

Additional file 1. Additional tables.

Additional file 2. Additional figures.

Abbreviations

3C: chromosome conformation capture; GAS: IFN γ activation site; IRF1: interferon regulatory factor 1; ISRE: interferon-stimulated response element; HAT: histone acetyltransferase; IFN γ : interferon- γ ; ISGs: IFN γ stimulated genes; esISGs: early strong induced ISGs; lsISGs: late strong induced ISGs; ewISGs: early weak induced ISGs; lwISGs: late weak induced ISGs; resISGs: resistant ISGs; potISGs: potential ISGs; IRGs: IFN γ repressed genes; lsIRGs: late strong IRGs; lwIRGs: late weak IRGs; SNPs: single nucleotide polymorphisms; STAT1: signal transducer and activator of transcription 1; TF: transcription factor; TSS: transcription start site.

Authors' contributions

MAEH generated and analyzed most of the data and KH performed most of the bioinformatics. MBKE and MAEH assessed TF binding in vitro, and were helped by AA. ZX helped with the bioinformatics. TY and ZN helped MAEH with ChIP. MS, MA, and IL helped generate reagents and analyze data. RB obtained funding, analyzed data, and wrote the paper with MAEH and KH. All authors read and approved the manuscript.

Author details

¹ Lunenfeld Tanenbaum Research Institute, Mt Sinai Hospital, Toronto, ON, Canada. ² Clinical Chemistry Division, Provincial Laboratory Services, Queen Elizabeth Hospital, Charlottetown, PE, Canada. ³ Department of Pathology, Faculty of Medicine, Dalhousie University, Halifax, NS, Canada. ⁴ Department of Lab Medicine and Pathobiology, University of Toronto, Toronto, ON, Canada. ⁵ Department of Ophthalmology and Vision Science, University of Toronto, Toronto, ON, Canada. ⁶ Present Address: Donnelly Centre, University of Toronto, Toronto, ON, Canada.

Acknowledgements

We thank Malcolm Macleod for designing the software to create TF binding maps.

Funding was provided by Canadian Institutes of Health Research (Grant No. MOP 111004); Canadian Cancer Society Research Institute (Grant No. 703079).

Competing interests

The authors declare that they have no competing interests.

Availability of data and materials

All data generated or analysed during this study are included in this published article and its Additional files 1 and 2, or will be submitted to GEO prior to publication.

Funding

This work was funded by grants to R.B. from the Canadian Cancer Society Research Institute (CCSR), the Canadian Health Research Institutes (CIHR), and the Krembil Foundation.

Received: 20 December 2016 Accepted: 2 March 2017

Published online: 09 March 2017

References

- Vesely MD, Kershaw MH, Schreiber RD, Smyth MJ. Natural innate and adaptive immunity to cancer. *Annu Rev Immunol*. 2011;29:235–71.
- Maher SG, Romero-Weaver AL, Scarzello AJ, Gamero AM. Interferon: cellular executioner or white knight? *Curr Med Chem*. 2007;14:1279–89.
- Hartman SE, Bertone P, Nath AK, Royce TE, Gerstein M, Weissman S, et al. Global changes in STAT target selection and transcription regulation upon interferon treatments. *Genes Dev*. 2005;19:2953–68.
- Robertson G, Hirst M, Bainbridge M, Bilenky M, Zhao Y, Zeng T, et al. Genome-wide profiles of STAT1 DNA association using chromatin immunoprecipitation and massively parallel sequencing. *Nat Methods*. 2007;4:651–7.
- Robertson AG, Bilenky M, Tam A, Zhao Y, Zeng T, Thiessen N, et al. Genome-wide relationship between histone H3 lysine 4 mono- and tri-methylation and transcription factor binding. *Genome Res*. 2008;18:1906–17.
- Au-Yeung N, Mandhana R, Horvath CM. Transcriptional regulation by STAT1 and STAT2 in the interferon JAK-STAT pathway. *JAK-STAT*. 2013;2:e23931.
- Ni Z, Abou El Hassan M, Xu Z, Yu T, Bremner R. The chromatin-remodeling enzyme BRG1 coordinates CIITA induction through many interdependent distal enhancers. *Nat Immunol*. 2008;9:785–93.
- Abou El Hassan M, Bremner R. A rapid simple approach to quantify chromosome conformation capture. *Nucleic Acids Res*. 2009;37:e35.
- Harismendy O, Notani D, Song X, Rahim NG, Tanasa B, Heintzman N, et al. 9p21 DNA variants associated with coronary artery disease impair interferon- γ signalling response. *Nature*. 2011;470:264–8.
- Ning S, Huye LE, Pagano JS. Regulation of the transcriptional activity of the IRF7 promoter by a pathway independent of interferon signaling. *J Biol Chem*. 2005;280:12262–70.
- Schroder K, Hertzog PJ, Ravasi T, Hume DA. Interferon-gamma: an overview of signals, mechanisms and functions. *J Leukoc Biol*. 2004;75:163–89.
- Pattenden SG, Klose R, Karaskov E, Bremner R. Interferon-gamma-induced chromatin remodeling at the CIITA locus is BRG1 dependent. *EMBO J*. 2002;21:1978–86.
- Abou El Hassan M, Yu T, Song L, Bremner R. Polycomb repressive complex 2 confers BRG1 dependency on the CIITA locus. *J Immunol*. 2015;194:5007.
- Morris AC, Beresford GW, Mooney MR, Boss JM. Kinetics of a gamma interferon response: expression and assembly of CIITA promoter IV and inhibition by methylation. *Mol Cell Biol*. 2002;22:4781–91.
- Ramsauer K, Farlik M, Zupkovic G, Seiser C, Kröger A, Hauser H, et al. Distinct modes of action applied by transcription factors STAT1 and IRF1 to initiate transcription of the IFN-gamma-inducible gbp2 gene. *Proc Natl Acad Sci USA*. 2007;104:2849–54.
- Shi L, Perin JC, Leipzig J, Zhang Z, Sullivan KE. Genome-wide analysis of interferon regulatory factor 1 binding in primary human monocytes. *Gene*. 2011;487:21–8.
- Frontini M, Vijayakumar M, Garvin A, Clarke N. A ChIP-chip approach reveals a novel role for transcription factor IRF1 in the DNA damage response. *Nucleic Acids Res*. 2009;37:1073–85.
- Rettno A, Clarke NM. Genome-wide identification of IRF1 binding sites reveals extensive occupancy at cell death associated genes. *J Carcinog Mutagen*. 2013;(Spec Iss Apoptosis):S6–009.
- Xie D, Boyle AP, Wu L, Zhai J, Kawli T, Snyder M. Dynamic trans-acting factor colocalization in human cells. *Cell*. 2013;155:713–24.
- Kumatori A, Yang D, Suzuki S, Nakamura M. Cooperation of STAT-1 and IRF-1 in interferon-gamma-induced transcription of the gp91 (phox) gene. *J Biol Chem*. 2002;277:9103–11.
- Chatterjee-Kishore M, Wright KL, Ting JP, Stark GR. How Stat1 mediates constitutive gene expression: a complex of unphosphorylated Stat1 and IRF1 supports transcription of the LMP2 gene. *EMBO J*. 2000;19:4111–22.
- Heintzman ND, Hon GC, Hawkins RD, Kheradpour P, Stark A, Harp LF, et al. Histone modifications at human enhancers reflect global cell-type-specific gene expression. *Nature*. 2009;459:108–12.
- Sung PS, Cheon H, Cho CH, Hong S-H, Park DY, Seo H-I, et al. Roles of unphosphorylated ISGF3 in HCV infection and interferon responsiveness. *Proc Natl Acad Sci USA*. 2015;112:10443–8.
- Cheon H, Stark GR. Unphosphorylated STAT1 prolongs the expression of interferon-induced immune regulatory genes. *Proc Natl Acad Sci USA*. 2009;106:9373–8.
- Reich NC, Liu L. Tracking STAT nuclear traffic. *Nat Rev Immunol*. 2006;6:602–12.
- Lödige I, Marg A, Wiesner B, Malecová B, Oelgeschläger T, Vinkemeier U. Nuclear export determines the cytokine sensitivity of STAT transcription factors. *J Biol Chem*. 2005;280:43087–99.
- Vinkemeier U. Getting the message across, STAT! Design principles of a molecular signaling circuit. *J Cell Biol*. 2004;167:197–201.
- Meyer T, Marg A, Lemke P, Wiesner B, Vinkemeier U. DNA binding controls inactivation and nuclear accumulation of the transcription factor Stat1. *Genes Dev*. 2003;17:1992–2005.
- Majoros A, Platanitis E, Szappanos D, Cheon H, Vogl C, Shukla P, et al. Response to interferons and antibacterial innate immunity in the absence of tyrosine-phosphorylated STAT1. *EMBO Rep*. 2016;17:367–82.
- White LC, Wright KL, Felix NJ, Ruffner H, Reis LF, Pine R, et al. Regulation of LMP2 and TAP1 genes by IRF-1 explains the paucity of CD8+ T cells in IRF-1 $-/-$ mice. *Immunity*. 1996;5:365–76.
- Dimitriou ID, Clemenza L, Scotter AJ, Chen G, Guerra FM, Rottapel R. Putting out the fire: coordinated suppression of the innate and adaptive immune systems by SOCS1 and SOCS3 proteins. *Immunol Rev*. 2008;224:265–83.
- Wu J, Ma C, Wang H, Wu S, Xue G, Shi X, et al. A MyD88-JAK1-STAT1 complex directly induces SOCS-1 expression in macrophages infected with Group A Streptococcus. *Cell Mol Immunol*. 2015;12:373–83.
- Heintzman ND, Stuart RK, Hon G, Fu Y, Ching CW, Hawkins RD, et al. Distinct and predictive chromatin signatures of transcriptional promoters and enhancers in the human genome. *Nat Genet*. 2007;39:311–8.
- Wright KL, Ting JP. Epigenetic regulation of MHC-II and CIITA genes. *Trends Immunol*. 2006;27:405–12.
- Ni Z, Karaskov E, Yu T, Callaghan SM, Der S, Park DS, et al. Apical role for BRG1 in cytokine-induced promoter assembly. *Proc Natl Acad Sci USA*. 2005;102:14611–6.
- Chou SD, Khan AN, Magner WJ, Tomasi TB. Histone acetylation regulates the cell type specific CIITA promoters, MHC class II expression and antigen presentation in tumor cells. *Int Immunol*. 2005;17:1483–94.
- Collinge M, Pardi R, Bender JR. Class II transactivator-independent endothelial cell MHC class II gene activation induced by lymphocyte adhesion. *J Immunol*. 1998;161:1589–93.
- Zhou H, Su HS, Zhang X, Douhan J rd, Glimcher LH. CIITA-dependent and -independent class II MHC expression revealed by a dominant negative mutant [In Process Citation]. *J Immunol*. 1997;158:4741–9.
- Magner WJ, Kazim AL, Stewart C, Romano MA, Catalano G, Grande C, et al. Activation of MHC class I, II, and CD40 gene expression by histone deacetylase inhibitors. *J Immunol*. 1990;145(165):7017–24.
- Guerra SG, Vyse TJ, Cunninghame Graham DS. The genetics of lupus: a functional perspective. *Arthritis Res Ther*. 2012;14:211.
- Kim H-J, Eom C-Y, Kwon J, Joo J, Lee S, Nah S-S, et al. Roles of interferon-gamma and its target genes in schizophrenia: proteomics-based reverse genetics from mouse to human. *Proteomics*. 2012;12:1815–29.
- Kantarci OH, Hebrink DD, Schaefer-Klein J, Sun Y, Achenbach S, Atkinson EJ, et al. Interferon gamma allelic variants: sex-biased multiple sclerosis susceptibility and gene expression. *Arch Neurol*. 2008;65:349–57.
- Cooke GS, Campbell SJ, Sillah J, Gustafson P, Bah B, Sirugo G, et al. Polymorphism within the interferon-gamma/receptor complex is associated with pulmonary tuberculosis. *Am J Respir Crit Care Med*. 2006;174:339–43.
- Thye T, Burchard GD, Nilius M, Müller-Myhsok B, Horstmann RD. Genomewide linkage analysis identifies polymorphism in the human interferon-gamma receptor affecting Helicobacter pylori infection. *Am J Hum Genet*. 2003;72:448–53.

45. Grant SFA, Hakonarson H. Microarray technology and applications in the arena of genome-wide association. *Clin Chem*. 2008;54:1116–24.
46. Dogan N, Wu W, Morrissey CS, Chen K-B, Stonestrom A, Long M, et al. Occupancy by key transcription factors is a more accurate predictor of enhancer activity than histone modifications or chromatin accessibility. *Epigenetics Chromatin*. 2015;8:16.
47. Jin F, Li Y, Dixon JR, Selvaraj S, Ye Z, Lee AY, et al. A high-resolution map of the three-dimensional chromatin interactome in human cells. *Nature*. 2013;503:290–4.
48. Andersson R, Gebhard C, Miguel-Escalada I, Hoof I, Bornholdt J, Boyd M, et al. An atlas of active enhancers across human cell types and tissues. *Nature*. 2014;507:455–61.
49. Ellinghaus D, Ellinghaus E, Nair RP, Stuart PE, Esko T, Metspalu A, et al. Combined analysis of genome-wide association studies for Crohn disease and psoriasis identifies seven shared susceptibility loci. *Am J Hum Genet*. 2012;90:636–47.
50. Nicolae DL, Gamazon E, Zhang W, Duan S, Dolan ME, Cox NJ. Trait-associated SNPs are more likely to be eQTLs: annotation to enhance discovery from GWAS. *PLoS Genet*. 2010;6:e1000888.
51. Zhong H, Beaulaurier J, Lum PY, Molony C, Yang X, Macneil DJ, et al. Liver and adipose expression associated SNPs are enriched for association to type 2 diabetes. *PLoS Genet*. 2010;6:e1000932.
52. Franke A, McGovern DPB, Barrett JC, Wang K, Radford-Smith GL, Ahmad T, et al. Genome-wide meta-analysis increases to 71 the number of confirmed Crohn's disease susceptibility loci. *Nat Genet*. 2010;42:1118–25.
53. International Genetics of Ankylosing Spondylitis Consortium (IGAS), Cortes A, Hadler J, Pointon JP, Robinson PC, Karaderi T, et al. Identification of multiple risk variants for ankylosing spondylitis through high-density genotyping of immune-related loci. *Nat Genet*. 2013;45:730–8.
54. Ricaño-Ponce I, Wijmenga C. Mapping of immune-mediated disease genes. *Annu Rev Genomics Hum Genet*. 2013;14:325–53.
55. Maurano MT, Humbert R, Rynes E, Thurman RE, Haugen E, Wang H, et al. Systematic localization of common disease-associated variation in regulatory DNA. *Science*. 2012;337:1190–5.
56. Schaub MA, Boyle AP, Kundaje A, Batzoglu S, Snyder M. Linking disease associations with regulatory information in the human genome. *Genome Res*. 2012;22:1748–59.
57. Bolstad BM, Irizarry RA, Astrand M, Speed TP. A comparison of normalization methods for high density oligonucleotide array data based on variance and bias. *Bioinform Oxf Engl*. 2003;19:185–93.
58. Hollander M, Wolfe DA. Nonparametric statistical methods, solutions manual. 2nd ed. New York: Wiley. <http://www.wiley.com/WileyCDA/WileyTitle/productCd-047132986X.html>. Accessed 6 Dec 2016.
59. Chen D, Pacal M, Wenzel P, Knoepfler PS, Leone G, Bremner R. Division and apoptosis of E2f-deficient retinal progenitors. *Nature*. 2009;462:925–9.

Submit your next manuscript to BioMed Central and we will help you at every step:

- We accept pre-submission inquiries
- Our selector tool helps you to find the most relevant journal
- We provide round the clock customer support
- Convenient online submission
- Thorough peer review
- Inclusion in PubMed and all major indexing services
- Maximum visibility for your research

Submit your manuscript at
www.biomedcentral.com/submit

